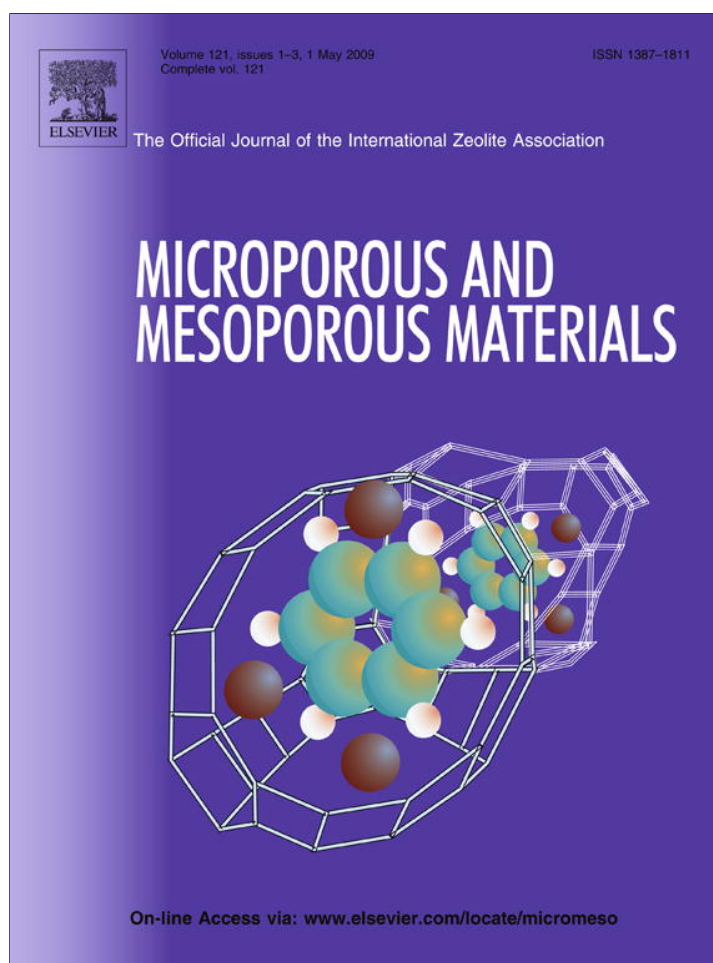


Provided for non-commercial research and education use.
Not for reproduction, distribution or commercial use.



This article appeared in a journal published by Elsevier. The attached copy is furnished to the author for internal non-commercial research and education use, including for instruction at the authors institution and sharing with colleagues.

Other uses, including reproduction and distribution, or selling or licensing copies, or posting to personal, institutional or third party websites are prohibited.

In most cases authors are permitted to post their version of the article (e.g. in Word or Tex form) to their personal website or institutional repository. Authors requiring further information regarding Elsevier's archiving and manuscript policies are encouraged to visit:

<http://www.elsevier.com/copyright>



Contents lists available at ScienceDirect

Microporous and Mesoporous Materials

journal homepage: www.elsevier.com/locate/micromeso

Thermally stable luminescent lanthanide complexes in zeolite L

Yige Wang^a, Huanrong Li^{a,*}, Lijian Gu^a, Quanying Gan^a, Yanni Li^b, Gion Calzaferri^{c,*}^a School of Chemical Engineering and Technology, Tianjin 300130, PR China^b School of Chemical Engineering and Technology, Tianjin University, Tianjin 300072, PR China^c Department of Chemistry and Biochemistry, University of Bern, Freiestrasse 3, CH-3012 Bern, Switzerland

ARTICLE INFO

Article history:

Received 14 August 2008

Received in revised form 21 November 2008

Accepted 19 December 2008

Available online 11 January 2009

Keywords:

Host-guest

Lanthanide

Luminescence

Zeolite L

FRET

Organolanthanide

ABSTRACT

Organolanthanide complexes inside the nanochannels of zeolite L crystals have been synthesized using a ship in a bottle procedure by inserting 2,2-bipyridine (bpy) from gas phase into the nanochannels of Ln³⁺-zeolite L crystals; Ln³⁺ = Tb³⁺ or Eu³⁺. The resulting Ln³⁺(bpy)_n-zeolite L host-guest materials were characterized by FT-IR and photoluminescence spectroscopy, by thermogravimetry and by SEM. The encapsulated luminescent organolanthanide complexes show remarkably increased thermal stability.

© 2008 Elsevier Inc. All rights reserved.

1. Introduction

Zeolites can host a great variety of photochemically and photo-physically active guests. Therefore, they have attracted considerable interest for constructing novel materials designed at nanosize level and they are of particular interest in the area of optical materials where predefined distances or a specific spatial pattern of the guests is required to obtain a desired optical response [1–12]. It has been shown that zeolite L is a very suitable host for developing functional host-guest materials [13–19]. It is a crystalline aluminosilicate in which corner-sharing SiO₄ and AlO₄ tetrahedra produce one-dimensional channels arranged in a hexagonal structure as shown in Fig. 1 [20–23]. The channels have a smallest free diameter of about 0.71 nm, the largest diameter inside is 1.26 nm. The distance between the centers of two neighbouring channels is 1.84 nm. They can be filled with suitable organic guest molecules. The number of channels lying parallel to the *c*-axis is $0.265(d_c)^2$, where d_c is the diameter of the cylinder in nanometer. This means that a crystal with a 550 nm diameter consists of about 8×10^4 strictly parallel channels. Many different guest species, including neutral and cationic organic dyes, have been incorporated into the one-dimensional channels of zeolite L

crystals. Photonic antenna materials have been obtained by inserting two or three different type of dyes where the donors are either located in the middle of the zeolite channels and the acceptors at the end or vice versa [18,19,24–26].

Organolanthanide complexes are well-known molecular luminescent materials, which possess characteristic narrow emission bands and long luminescence lifetimes. The optical transitions of the lanthanide Ln³⁺ ions involve 4f orbitals which are well shielded from the chemical environment by 5s² and 5p⁶ electrons. The f–f transitions are parity forbidden and, as a result, the absorption coefficients are very small and the emissive rates are slow. This results in long-lived excited states and line like emission bands. As a consequence, direct excitation of the Ln³⁺ ions is unfavorable. Different ways to overcome the difficulties of low absorptivity have been used [27]. A ligand centered absorption followed by energy transfer to the Ln³⁺ ions is a common way used for organolanthanides. This mechanism is often referred to as antenna effect. Such complexes have attracted interest in technological applications including optoelectronic devices and flat panel displays [28–33]. A few reports concern different Ln³⁺ species, including organolanthanides, embedded in zeolites, mainly Faujasites [2,11,34–37]. Little attention has been paid to the insertion of organolanthanide complexes into the channels of zeolite L, despite of the fact that zeolite L seems currently to be the only nanochannel material that can be synthesized in a size range starting from about 30 nm up to several thousand nm and with crystals of different morphology ranging from discs to elongated cylinders [38–40]. We recently reported preliminary results regarding supramolecular

* Corresponding authors. Tel.: +86 226020044; fax: +86 2226564294 (H. Li), tel.: +41 31 631 42 36; fax: +41 31 631 39 94 (G. Calzaferri).

E-mail addresses: lihuanrong@hebut.edu.cn (H. Li), gion.calzaferri@iac.unibe.ch (G. Calzaferri).

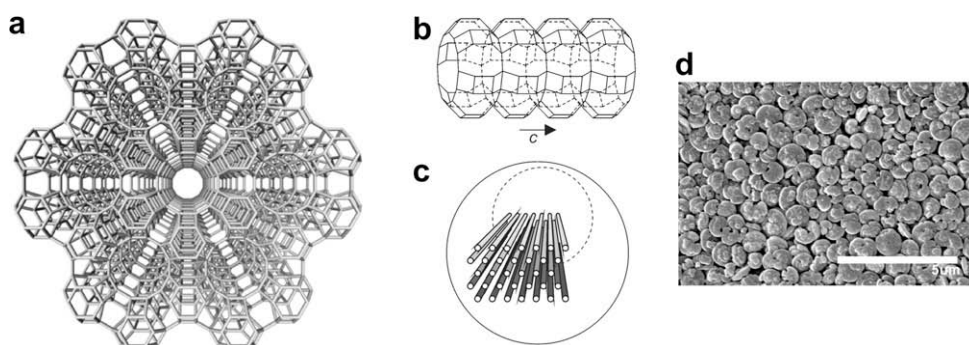


Fig. 1. Zeolite L. (a) top view of the framework of zeolite L, illustrating the hexagonal structure by showing a channel surrounded by six neighbouring channels. (b) Side view of a channel that consists of 0.75 nm long unit cells with a van der Waals opening of 0.71 nm at the smallest and 1.26 nm at the widest place. (c) Schematic view of the channels, shown as strictly parallel tubes. The center to center distance between two channels is 1.84 nm. (d) SEM image of the zeolite L crystals used in this work.

incorporation of lanthanide ions and an organic ligand into the channels of zeolite L. The material was prepared by reacting 1,10-phenanthroline or benzophenone with Eu^{3+} -zeolite L [41,42]. This kind of syntheses has been known as “ship in a bottle” method and was pioneered by Lundsford et al. in the early 1980s [43]. Since it has been used successfully for preparing many different materials [23,44]. The name is due to artistic bottle containing a ship that is larger than the bottle neck.

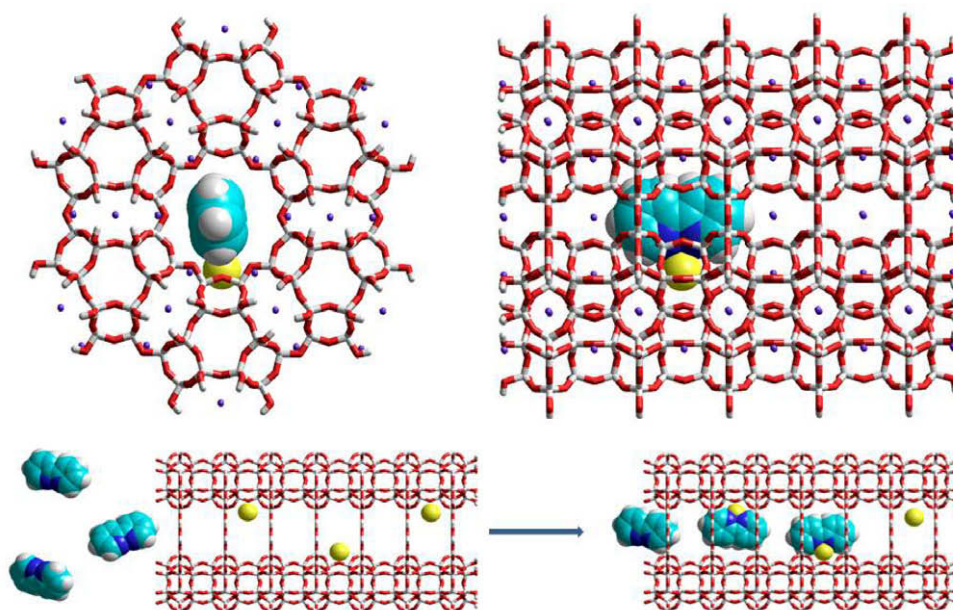
We report the synthesis of $\text{Ln}^{3+}(\text{bpy})_n$ -zeolite L ($\text{Ln}^{3+} = \text{Tb}^{3+}$ or Eu^{3+}) materials, investigate their luminescence properties and stability, and we discuss consequences of our findings.

2. Experimental

2.1. Materials

Zeolite L was synthesized according to a previously reported procedure using a start mixture of the composition $5.40 \text{ K}_2\text{O}-5.50 \text{ Na}_2\text{O}-1.00 \text{ Al}_2\text{O}_3-30.00 \text{ SiO}_2-416.08 \text{ H}_2\text{O}$ [40]. The resulting

zeolite L crystals had an average length and diameter of 300 and 800 nm, respectively. The potassium exchanged form was used. 2,2-bipyridine (bpy) was purchased from Aldrich and used as received. $\text{TbCl}_3 \cdot 6\text{H}_2\text{O}$ and $\text{EuCl}_3 \cdot 6\text{H}_2\text{O}$ were obtained by dissolving Tb_4O_7 and Eu_2O_3 in hydrochloric acid (37%). The $\text{Ln}(\text{bpy})_2\text{Cl}_3 \cdot 2\text{H}_2\text{O}$ complexes were synthesized by the procedure reported in Ref. [45]. The Ln^{3+} -zeolite L samples were prepared by ion-exchange. An appropriate amount of zeolite L was stirred in an aqueous solution of $\text{LnCl}_3 \cdot 6\text{H}_2\text{O}$ ($\text{Ln}^{3+} = \text{Tb}^{3+}$ or Eu^{3+}). Typically 50 mg of zeolite L was added to 10 mL of a 0.05 molar aqueous solution of $\text{LnCl}_3 \cdot 6\text{H}_2\text{O}$ and stirred for 16 h at 353 K. The products were collected by centrifugation, washed with deionized water, and dried in air at 353 K. The organolanthanide-zeolite L materials $\text{Ln}^{3+}(\text{bpy})_n$ -zeolite L were synthesized by using the ship in a bottle method [43,44]. The Ln^{3+} -zeolite L samples were degassed and dried for 1 h at 423 K and then kept in contact with the vapor of bpy at 393 K overnight. The resulting material was washed with CH_2Cl_2 , in order to remove only physically adsorbed ligand, and dried at 40 °C in vacuum for 6 h.



Scheme 1. Ship-in-bottle synthesis procedure. The upper part of this scheme shows a front and a side view of the structure of zeolite L with a $\text{Ln}^{3+}(\text{bpy})$; the Ln^{3+} ion is yellow. The violet balls are the potassium cations that belong to the zeolite. Monovalent cations of 3.6 per unit cell can be exchanged. Water molecules are not shown. The lower part illustrates the synthesis procedure. bpy enters the channels, shown in a simplified way, to form the complex. The scheme also illustrates that the reaction is easier and faster close to the channel ends. Space restriction makes it more difficult for the ligand to reach the Ln^{3+} ions lying deeper inside. (For interpretation of the references to colour in this scheme legend, the reader is referred to the web version of this article.)

2.2. Characterization

Infrared (IR) spectra were obtained on a Bruker Vector 22 spectrometer in the range of 400–4000 cm^{-1} at a resolution of 4 cm^{-1} (16 scans were collected). About 2 mg of the sample was mixed with potassium bromide (Merck, spectroscopic grade), finely ground and pressed into pellets. Thermogravimetry (TGA) was performed using a SDT-TG Q 600, TA Instrument. In the TGA experiments the samples were analyzed from r.t. up to 800 $^{\circ}\text{C}$ at a heating rate of 10 $^{\circ}\text{C min}^{-1}$ with air as purging gas. SEM images were obtained using a FE-SEM (Hitachi S-4300) at an acceleration voltage of 10 kV. The steady-state luminescence spectra and the lifetimes were measured on an Edinburgh Instrument FS920P spectrometer, with a 450 W xenon lamp as the steady-state excitation source, a double excitation monochromator (1800 lines mm^{-1}), an emission monochromator (600 lines mm^{-1}), and a semiconductor cooled Hamamatsu RMP928 photomultiplier tube. The samples were deposited as powder on a quartz plate and measured under ambient conditions.

3. Results and discussion

An SEM image of the zeolite used in this study is shown in Fig. 1d. It illustrates the disc-shaped form of the crystals which had a length between 200 and 400 nm and a diameter in the order of 800 nm. The stoichiometry of zeolite L is $(\text{M}^+)_{\text{g}}[(\text{AlO}_2)_{\text{g}}(\text{SiO}_2)_{27}] \times n\text{H}_2\text{O}$, where M^+ are monovalent cations (violet balls in Scheme 1) compensating the negative charge resulting from the aluminium atoms. Here, n is 21 in fully hydrated materials, and 16 at about 22% relative humidity. We used the potassium form. The Ln^{3+} ions were introduced by ion-exchange using an aqueous solution containing an excess of $\text{TbCl}_3 \cdot 6\text{H}_2\text{O}$ or $\text{EuCl}_3 \cdot 6\text{H}_2\text{O}$. The amount of exchanged Ln^{3+} ions per unit cell was found to be nearly 1, as determined by analyzing the supernatant (titration against EDTA). This is the maximum loading that can be expected, since 3.6 monovalent ions per u.c. can be exchanged. The choice of bpy as a ligand was based on the reported luminescence properties of the corresponding complexes in solution [45]. The syntheses of the $\text{Ln}^{3+}(\text{bpy})_n$ inside of the zeolite L nanochannels, which led to the $\text{Ln}^{3+}(\text{bpy})_n$ -zeolite L materials, was carried out according to the “ship in a bottle” method illustrated in Scheme 1. The ligand was allowed to enter the channels of the degassed and dried Ln^{3+} -zeolite L via gas-diffusion at 393 K. The amount of inserted bpy was about 0.65 per unit cell, as determined for the $\text{Eu}^{3+}(\text{bpy})_n$ -zeolite L materials by elemental analysis. This is a high loading and corresponds to a concentration of 0.5 mol/L. Formation of the lanthanide complex in the nanochannels was confirmed by the chemical properties of the material, by FT-IR spectroscopy, by thermogravimetry and by luminescence spectroscopy.

We report in Fig. 2, FT-IR spectra of an $\text{Eu}^{3+}(\text{bpy})_n$ -zeolite L sample. They are dominated by the very intense anti-symmetric $\nu_{\text{as}}(\text{T-O})$ stretching vibrations ($T = \text{Si}^{4+}$ or Al^{3+}) around 1100 cm^{-1} . The water molecules present in the sample are characterized by the stretching and the bending vibrations at about 3450 and 1640 cm^{-1} , respectively. The enlargement in Fig. 2b shows two well developed bands at 1438 and at 1534 cm^{-1} which are not present in absence of the ligand bpy. The former is in clear agreement with the formation of the $\text{Eu}^{3+}(\text{bpy})_n$ while the latter is due to protonation of the ligand, leading to bpyH^+ [34]. The acidity properties of zeolite L materials have been discussed recently in detail [46].

The thermal stability of the host-guest materials was studied by means of TGA. We report in Fig. 3, a comparison of the thermal stability of the free complex and of the host-guest materials. The TGA of $\text{Eu}^{3+}(\text{bpy})_n$ -zeolite L, in presence of air, is shown in

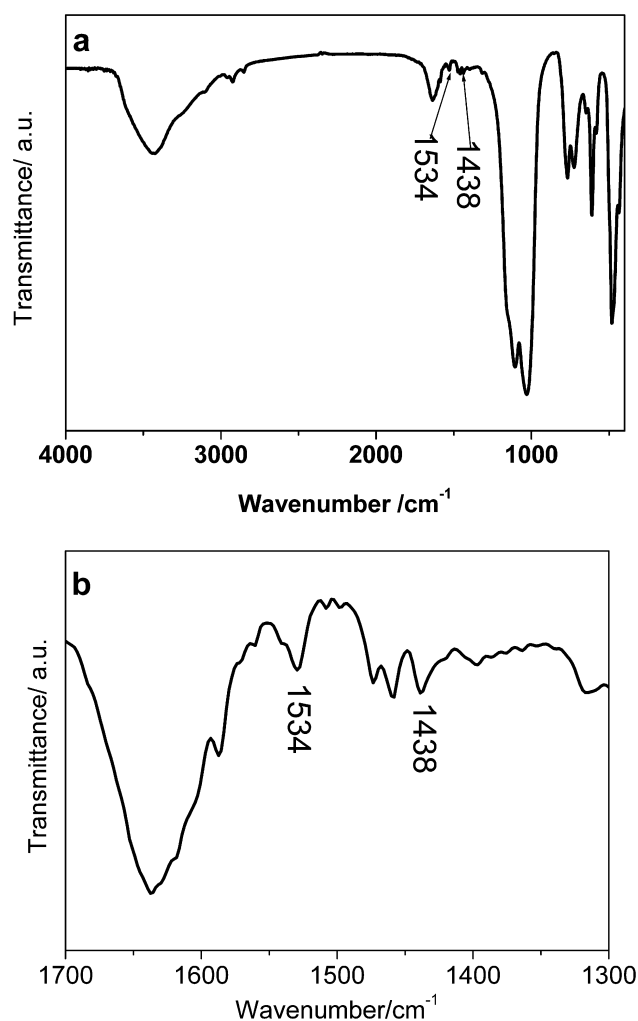


Fig. 2. FT-IR spectrum of an $\text{Eu}^{3+}(\text{bpy})_n$ -zeolite L sample and enlargement in the range of 1700–1300 cm^{-1} .

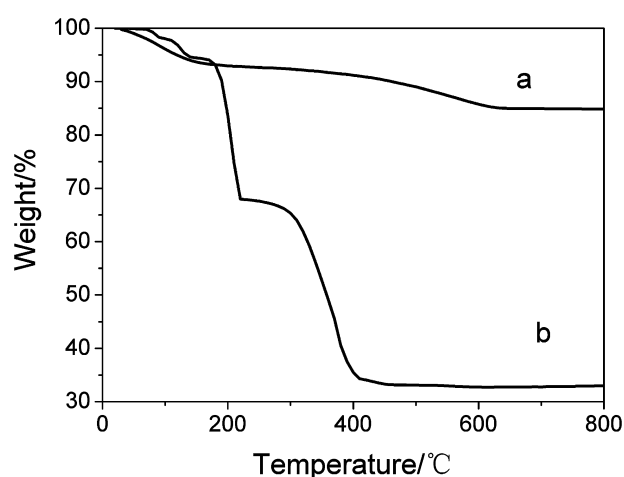


Fig. 3. Comparison of the thermal stability of the free complex and of the host-guest materials. (a) TGA of the $\text{Eu}^{3+}(\text{bpy})_n$ -zeolite L material, in presence of air. (b) TGA of $\text{Eu}^{3+}(\text{bpy})_2\text{Cl}_3 \cdot 2\text{H}_2\text{O}$, in presence of air.

Fig. 3a. We observe two weight loss steps. In the first step which ends at 200 $^{\circ}\text{C}$ a weight loss of about 7% occurs. In this process 95% of the water leaves the framework. It is known that the

remaining 5% water desorbs only reluctantly. The second step, with a weight loss of 8%, is first more gradual and related to a weight loss of 1% in the temperature range of 200–340 °C. It becomes faster above 400 °C, due to desorption and/or combustion of the bpy. This interpretation is supported by a comparison with the thermal analysis results reported for zeolite L and dye-loaded Zeolite L [26]. The TGA of $\text{Eu}^{3+}(\text{bpy})_2\text{Cl}_3 \cdot 2\text{H}_2\text{O}$, in presence of air, is shown in Fig. 3b. We observe three weight loss steps. At about 180 °C decomposition of the materials starts. This comparison impressively illustrates the large difference between the properties of the free complex and the host-guest material. We should add that $\text{Eu}^{3+}(\text{bpy})_n$ -zeolite L remains white after heating in air for 3 h at 400 °C.

Hydrated Ln^{3+} -zeolite L ($\text{Ln}^{3+} = \text{Tb}^{3+}$ or Eu^{3+}) materials show no obvious luminescence upon irradiation at 300 nm. The luminescence yield of Eu^{3+} -zeolite L is less than 1%. This is attributed to the coupling of the $\text{Eu}^{3+} \ ^5\text{D}_0$ state with high-energy vibrations of coordinated water which quenches the luminescence [47]. A large gain in luminescence intensity is observed after incorporation of bpy, which leads to the formation of $\text{Ln}^{3+}(\text{bpy})_n$ -zeolite L, as evidenced by the green and the red emission for Tb^{3+} and Eu^{3+} , respectively, upon irradiation at 300 nm. We compare in Fig. 4, the excitation and the luminescence spectra of $\text{Tb}^{3+}(\text{bpy})_n$ -zeolite L with those of $\text{Tb}^{3+}(\text{bipy})_2\text{Cl}_3 \cdot 2\text{H}_2\text{O}$, both deposited on a quartz plate and measured under ambient conditions, and in Fig. 5, the luminescence decay after excitation at 316 nm for $\text{Tb}^{3+}(\text{bpy})_n$ -zeolite L and 327 nm for $\text{Tb}^{3+}(\text{bipy})_2\text{Cl}_3 \cdot 2\text{H}_2\text{O}$. The excitation spectrum of zeolite $\text{Tb}^{3+}(\text{bpy})_n$ -zeolite L monitored at 544 nm is dominated by a broad band with two main components peaking at 254 nm and 316 nm, respectively; no f–f transitions can be observed. Excitation into the ligand at 316 nm results in a bright green line-shaped emission. The emissions bands are assigned to the transitions from the $^5\text{D}_4$ level to the $^7\text{F}_j$ levels ($j = 6, 5, 4, 3$) at 490, 544, 584, and 620 nm, respectively. No emission of the ligand is observed. This proves that the bpy ligands absorb the excitation energy and transfer it efficiently to the chelated Tb^{3+} ions. The half-width of the strongest bands is less than 15 nm, indicating that the $\text{Tb}^{3+}(\text{bpy})_n$ -zeolite L nano-composites exhibit high fluorescence intensity and color purity. The $\text{Tb}^{3+}(\text{bpy})_n$ -zeolite L material shows very similar spectral feature as the complex $\text{Tb}^{3+}(\text{bipy})_2\text{Cl}_3 \cdot 2\text{H}_2\text{O}$. No obvious shift in wavelength of the emission bands has been observed. The luminescence decay of $\text{Tb}^{3+}(\text{bpy})_n$ -zeolite L and $\text{Tb}^{3+}(\text{bipy})_2\text{Cl}_3 \cdot 2\text{H}_2\text{O}$ was measured under excitation at 316 nm and 327 nm, respectively. It follows a single-exponential function with lifetimes of the $^5\text{D}_4$ state of 0.737 ms and 0.705 ms for $\text{Tb}^{3+}(\text{bipy})_2\text{Cl}_3 \cdot 2\text{H}_2\text{O}$ and $\text{Tb}^{3+}(\text{bpy})_n$ -zeolite L, respectively.

A good method to investigate and to compare the thermal stability of $\text{Tb}^{3+}(\text{bpy})_n$ -zeolite L and $\text{Tb}^{3+}(\text{bipy})_2\text{Cl}_3 \cdot 2\text{H}_2\text{O}$ is to study their luminescence behavior upon heat treatment. We show in Fig. 6, the luminescence spectra of both sample heated in air at 400 °C for 3 h. The emission spectra were obtained upon excitation at 320 nm. We observe that after this treatment $\text{Tb}^{3+}(\text{bpy})_n$ -zeolite L still exhibits white color and displays the green emission with the characteristic four strong and narrow lines. In the pure $\text{Tb}^{3+}(\text{bipy})_2\text{Cl}_3 \cdot 2\text{H}_2\text{O}$ complex, most of the narrow lines disappeared and a new narrow line at 467 nm and a broad band centered at 660 nm evolved. The narrow line can be ascribed to the $^5\text{D}_3 \rightarrow ^7\text{F}_6$ transition, while the origin of the broad band is unclear. A quantitative comparison with samples treated at 150 °C for 3 h, which results in the best emitting material we have obtained, showed that $\text{Tb}^{3+}(\text{bpy})_n$ -zeolite L lost only 20% of its emission intensity upon the 3 h lasting treatment at 400 °C. This demonstrates the marked enhancement of thermal stability of the encapsulated organolanthanide complex.

The Tb^{3+} can be replaced by Eu^{3+} that shows bright red luminescence. The excitation and the luminescence spectra of $\text{Eu}^{3+}(\text{bpy})_n$ -

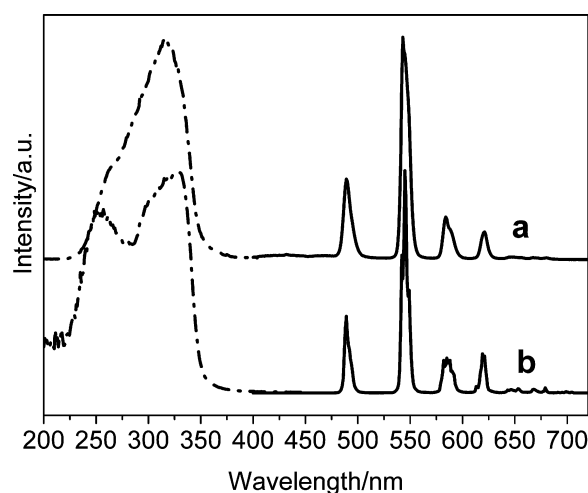


Fig. 4. Excitation (dash-dot line) and luminescence spectra (solid line): (a) $\text{Tb}^{3+}(\text{bpy})_n$ -zeolite L and (b) $\text{Tb}^{3+}(\text{bipy})_2\text{Cl}_3 \cdot 2\text{H}_2\text{O}$, both deposited on a quartz plate and measured under ambient conditions.

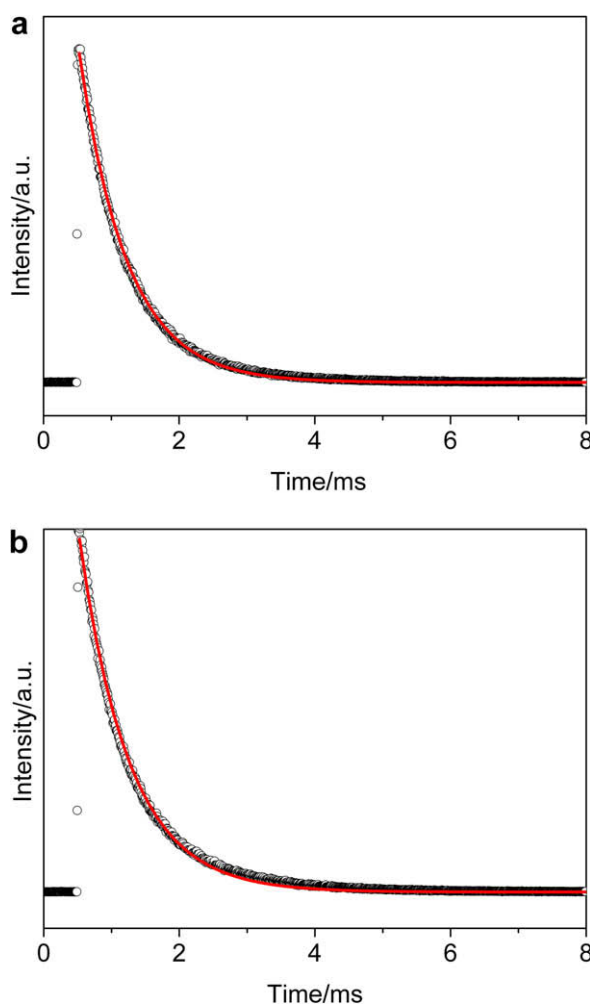


Fig. 5. Luminescence decay after excitation at 316 nm for $\text{Tb}^{3+}(\text{bpy})_n$ -zeolite L and 327 nm for $\text{Tb}^{3+}(\text{bipy})_2\text{Cl}_3 \cdot 2\text{H}_2\text{O}$: (a) $\text{Tb}^{3+}(\text{bpy})_n$ -zeolite L and (b) $\text{Tb}^{3+}(\text{bipy})_2\text{Cl}_3 \cdot 2\text{H}_2\text{O}$, both deposited on a quartz plate and measured under ambient conditions. The experimental data are shown as circles while the fitting result is shown as a solid line.

zeolite L and of $\text{Eu}^{3+}(\text{bpy})_2\text{Cl}_3 \cdot 2\text{H}_2\text{O}$ are reported in Fig. 7. As anticipated, the $\text{Eu}^{3+}(\text{bpy})_n$ -zeolite L material shows similar excitation

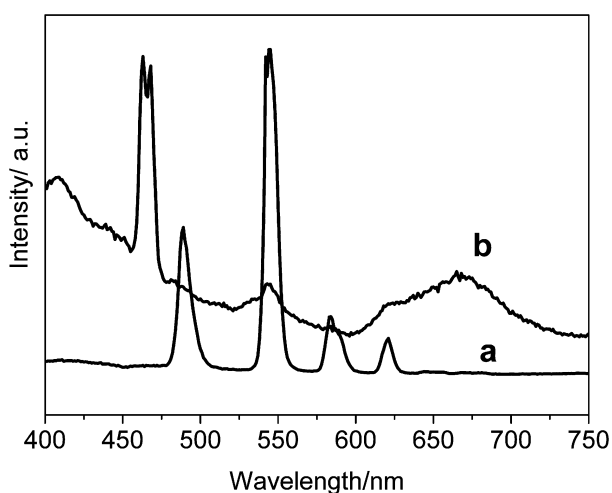


Fig. 6. Comparison of the luminescence spectra, recorded after treatment of the samples at 400 °C during 4 h. (a) $\text{Tb}^{3+}(\text{bpy})_n$ -zeolite L and (b) $\text{Tb}^{3+}(\text{bpy})_2\text{Cl}_3 \cdot 2\text{H}_2\text{O}$, both deposited on a quartz plate and measured under ambient conditions.

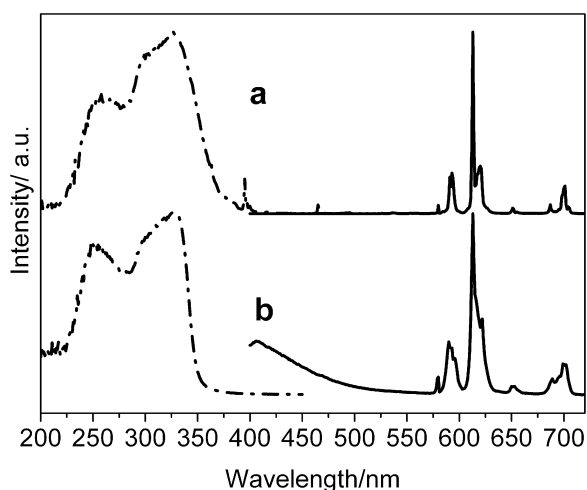


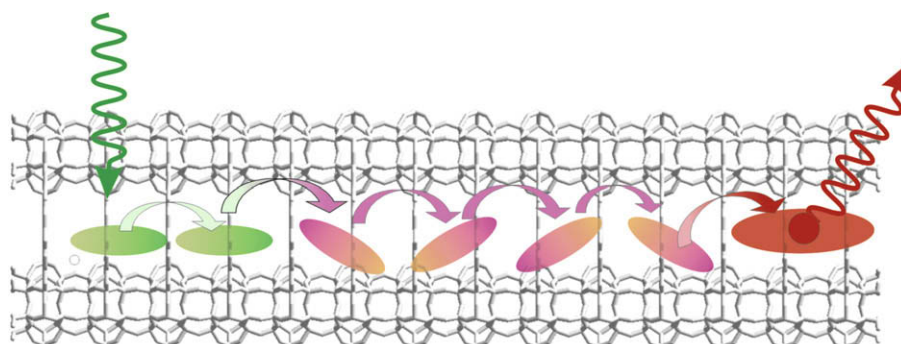
Fig. 7. Excitation (dotted line) and emission spectra (solid line). (a) $\text{Eu}^{3+}(\text{bpy})_2\text{Cl}_3 \cdot 2\text{H}_2\text{O}$ and (b) $\text{Eu}^{3+}(\text{bpy})_n$ -zeolite L, both deposited on a quartz plate and measured under ambient conditions.

and emission spectral feature as the $\text{Eu}^{3+}(\text{bipy})_2\text{Cl}_3 \cdot 2\text{H}_2\text{O}$ complex. The broad band in the excitation spectra can be assigned to absorption of the ligand. The five prominent emission peaks at 579, 593, 612, 650, and 698 nm in the emission spectra can be

attributed to ${}^5\text{D}_0 \rightarrow {}^7\text{F}_j$ ($J = 0-4$) transitions, with the red emission for $J=2$ as the dominant feature. The fine splitting of the ${}^5\text{D}_0 \rightarrow {}^7\text{F}_2$ transition into distinct crystal field components indicates a 'crystalline' Eu^{3+} environment. It proves that the bpy europium complex is formed inside the nanochannel of zeolite L [48]. The single line of the ${}^5\text{D}_0 \rightarrow {}^7\text{F}_0$ transition, the local-field splitting of the ${}^7\text{F}_{1,2}$ levels, and the higher intensity of the ${}^5\text{D}_0 \rightarrow {}^7\text{F}_2$ transition indicate that the local Eu^{3+} coordination site is of low symmetry without an inversion center [49]. The high intensity of the ${}^5\text{D}_0 \rightarrow {}^7\text{F}_2$ line indicates that the actual coordination polyhedron is closer to a dodecahedron or a bicapped trigonal prism than to a square anti-prism [50,51]. In fact, no ${}^5\text{D}_0 \rightarrow {}^7\text{F}_2$ lines are expected for a Eu^{3+} in a square anti-prism environment [52]. The broad band of $\text{Eu}^{3+}(\text{bpy})_n$ -zeolite L at about 410 nm is due to an emission of the ligand. This indicates that the energy transfer from the bpy to Eu^{3+} ion is less efficient than in case of the $\text{Tb}^{3+}(\text{bpy})_n$ -zeolite L material.

4. Conclusions

Upon gas-phase insertion of bpy into Eu^{3+} or Tb^{3+} exchanged zeolite L crystals, a striking increase of the Eu^{3+} and of the Tb^{3+} emission occurs, as a consequence of the formation of $\text{Ln}^{3+}(\text{bpy})_n$ complexes inside the nanochannel. The encapsulation results in a marked enhancement of the thermal stability of the complexes. The new host-guest materials are suited to cooperation with UV-emitting LEDs because they can be excited in the near UV region. Furthermore, these materials can be tested for fabrication of different plastic photonic devices based on the recently published procedure of realizing transparent zeolite-polymer hybrid materials by means of a suitable functionalization of the external surfaces [53]. Importantly, this finding can also be regarded as a first step towards the realization of antenna sensitized organolanthanide-zeolite L material, as illustrated in Scheme 2. In such a system, excitation takes place at short wavelengths, indicated by the green arrow; but also longer wavelength excitation is possible. The excitation energy is then transported by FRET as indicated until it reaches the organolanthanide complex where it excites the ligand which then transfers the electronic excitation energy to the lanthanide ion, indicated as red circle, which then emits according to its characteristics. Dyes and ligand have to be chosen such that FRET can take place. The organolanthanide complex can also be added in a stopcock like manner [18]. A similar scheme has already been experimentally realized based on fully organic chromophores, donors and acceptors, as reported in Ref. [24]. With an organolanthanide complex as emitter, all the specific characteristics of such chromophores can be integrated. This extends the field of applications of the so far known dye-zeolite antenna systems considerable and leads to fascinating functional supramolecular organic-inorganic-lanthanide hybrid materials.



Scheme 2. Illustration of an antenna sensitized dye-organolanthanide-zeolite L material.

Acknowledgments

This work is financially supported by Hebei University of Technology, the Key Project of Chinese Ministry of Education (208016), Ministry of Personal, People's Republic of China and Department of Personal, Hebei Province and Scientific program launched in 2008 by Hebei province (08965110D) and National Natural Science Foundation of China (No. 20871040).

References

- [1] G. Calzaferri, H.R. Li, D. Bruehwiler, *Chem. Eur. J.* 14 (2008) 7442.
- [2] M. Lezhnina, F. Laeri, L. Benmouhadi, U. Kynast, *Adv. Mater.* 18 (2006) 280.
- [3] D. Bruehwiler, G. Calzaferri, *Micropor. Mesopor. Mater.* 72 (2004) 1.
- [4] L. Tosheva, V.P. Valtchev, *Chem. Mater.* 17 (2005) 2494.
- [5] F. Laeri, F. Schueth, U. Simon, M. Wark (Eds.), *Host-Guest Systems Based on Nanoporous Crystals*, VCH, Weinheim, Germany, 2003.
- [6] M. Borja, P.K. Dutta, *Nature* 362 (1993) 43.
- [7] M.B.J. Roelfaers, R. Ameloot, Mukulesh Baruah, H. Uji-i, M. Bulut, G. De Cremer, U. Müller, P.A. Jacobs, J. Hofkens, B.F. Sels, D.E. De Vos, *J. Am. Chem. Soc.* 130 (2008) 5763.
- [8] M. Busby, C. Blum, M. Tibben, S. Fibikar, G. Calzaferri, V. Subramania, L. De Cola, *J. Am. Chem. Soc.* 130 (2008) 10970.
- [9] R. Xu, G. Zhu, X. Yin, X. Wan, S. Qiu, *J. Mater. Chem.* 16 (2006) 2200.
- [10] M. Ganschow, C. Hellriegel, E. Kneuper, M. Wark, C. Thiel, G. Schulz-Ekloff, C. Bräuchle, D. Wöhrle, *Adv. Funct. Mater.* 14 (2004) 269.
- [11] D. Sendor, U. Kynast, *Adv. Mater.* 14 (2002) 1570.
- [12] U. Vietze, O. Krauß, F. Laeri, G. Ihlein, F. Schueth, B. Limburg, M. Abraham, *Phys. Rev. Lett.* 81 (1998) 4628.
- [13] S. Hashimoto, K. Samata, T. Shoji, N. Taira, T. Tomita, S. Matsuo, *Micropor. Mesopor. Mater.* 117 (2009) 220.
- [14] M. Busby, H. Kerschbaumer, G. Calzaferri, L. De Cola, *Adv. Mater.* 20 (2008) 1614.
- [15] S. Hashimoto, H.R. Moon, K.B. Yoon, *Micropor. Mesopor. Mater.* 101 (2007) 10.
- [16] A. Zabala Ruiz, H.R. Li, G. Calzaferri, *Angew. Chem. Int. Ed.* 45 (2006) 5282.
- [17] H.R. Li, A. Devaux, Z. Popović, L. De Cola, G. Calzaferri, *Micropor. Mesopor. Mater.* 95 (2006) 112.
- [18] G. Calzaferri, S. Huber, H. Maas, C. Minkowski, *Angew. Chem. Int. Ed.* 42 (2003) 3732.
- [19] G. Calzaferri, M. Pauchard, H. Mass, S. Huber, A. Khatyr, T. Schaafsma, *J. Mater. Chem.* 12 (2002) 1.
- [20] D.W. Breck, *Zeolite Molecular Sieves*, Wiley, NY, 1974.
- [21] Ch. Baerlocher, W.M. Meier, D.H. Olson, *Atlas of Zeolite Framework Types*, fifth ed., Elsevier, Amsterdam, 2001.
- [22] T. Ohsuna, Y. Horikawa, K. Hiraga, O. Terasaki, *Chem. Mater.* 10 (1998) 688.
- [23] A. Corma, H. Garcia, *Eur. J. Inorg. Chem.* (2004) 1143.
- [24] G. Calzaferri, K. Lutkouskaya, *Photochem. Photobiol. Sci.* 7 (2008) 879.
- [25] C. Minkowski, R. Pansu, M. Takano, G. Calzaferri, *Adv. Funct. Mater.* 16 (2006) 273.
- [26] M. Pauchard, A. Devaux, G. Calzaferri, *Chem. Eur. J.* 6 (2000) 3456.
- [27] H. Maas, A. Currao, G. Calzaferri, *Angew. Chem. Int. Ed.* 41 (2002) 2495.
- [28] P. Escribano, B. Julián-López, J. Planelles-Aragó, E. Cordoncillo, B. Viana, C. Sanchez, *J. Mater. Chem.* 18 (2008) 23.
- [29] L. Song, X. Liu, Z. Zhen, C. Chen, D. Zhang, *J. Mater. Chem.* 17 (2007) 4586.
- [30] J.-C.G. Buenzli, C. Piguet, *Chem. Rev.* 102 (2002) 1897.
- [31] K.Y. Okamoto, *Chem. Rev.* 102 (2002) 2347.
- [32] H. Xin, M. Shi, X.M. Zhang, F.Y. Li, Z.Q. Bian, K. Ibrahim, F.Q. Liu, C.H. Huang, *Chem. Mater.* 15 (2003) 3728.
- [33] R.G. Denning, *J. Mater. Chem.* 11 (2001) 19.
- [34] M. Alvaro, V. Fornés, S. García, H. García, J.C. Scaiano, *J. Phys. Chem. B* 102 (1998) 8744.
- [35] Y. Wada, T. Okubo, M. Ryo, T. Nakazawa, H. Hasegawa, S. Yanagida, *J. Am. Chem. Soc.* 122 (2000) 8583.
- [36] Y. Wada, M. Sato, Y. Tsukahara, *Angew. Chem. Int. Ed.* 45 (2006) 1925.
- [37] I.L.V. Rosa, O.A. Serra, J.E. Nassar, *J. Lumin.* 72/74 (1997) 532.
- [38] Silke Megelski, Gion Calzaferri, *Adv. Funct. Mater.* 11 (2001) 277.
- [39] A. Zabala Ruiz, D. Bruehwiler, T. Ban, G. Calzaferri, *Monatshefte Fuer Chemie* 136 (2005) 77.
- [40] A. Zabala Ruiz, D. Brühwiler, L.Q. Dieu, G. Calzaferri, in: U. Schubert, N. Hüsing, R. Laine (Eds.), *Materials Syntheses, A Practical Guide*, Springer, Wien, 2008, pp. 9–19 (ISBN: 978-3-211-75124-4).
- [41] Y.G. Wang, Z. Guo, H.R. Li, *J. Rare Earths (Special Issue)* 25 (2007) 283.
- [42] A. Monguzzi, G. Macchi, F. Meinardi, R. Tubino, M. Burger, G. Calzaferri, *Appl. Phys. Lett.* 92 (2008) 123301.
- [43] W. DeWilde, G. Peeters, J.H. Lunsford, *J. Phys. Chem.* 84 (1980) 2306.
- [44] (a) P. Lainé, M. Lanz, G. Calzaferri, *Inorg. Chem.* 35 (1996) 3514;
(b) C. Leiggenger, G. Calzaferri, *ChemPhysChem* 5 (2004) 1593.
- [45] R.G. Charles, E.P. Riedel, P.G. Haverlack, *J. Chem. Phys.* 44 (1996) 1356.
- [46] R.Q. Albuquerque, G. Calzaferri, *Chem. Eur. J.* 13 (2007) 8939.
- [47] G. Stein, E. Wuerzberg, *J. Chem. Phys.* 62 (1975) 208.
- [48] M.H. Bartl, B.J. Scott, H.C. Huang, G. Wirnsberger, A. Popitsch, B.F. Chmelka, G.D. Stucky, *Chem. Commun.* (2002) 2474.
- [49] L.S. Fu, R.A.S. Ferreira, N.J.O. Silva, A.J. Fernandes, P. Ribeiro-Claro, I.S. Gonçalves, V. de Z. Bermudez, L.D. Carlos, *J. Mater. Chem.* 15 (2005) 3117.
- [50] K. Lunstroot, K. Driesen, P. Nockemann, C. Goerller-Walrand, K. Binnemans, S. Bellayer, J. Le Bideau, A. Vioux, *Chem. Mater.* 18 (2006) 5711.
- [51] C. Goeller-Walrand, K. Binnemans, *Rationalization of crystal field parametrization*, in: K. Gschneider, L. Eyring (Eds.), *Handbook on the Physics and Chemistry of Rare Earths*, vol. 23, Elsevier, Amsterdam, 1996, pp. 121–283 (Chapter 155).
- [52] G. Blasse, *Inorg. Chim. Acta* 142 (1988) 153.
- [53] S. Suárez, A. Devaux, J. Banuelos, O. Bossart, A. Kunzmann, G. Calzaferri, *Adv. Funct. Mater.* 17 (2007) 2298.